

Influence of Embedded Nanocontainers on the Efficiency of Active Anticorrosive Coatings for Aluminum Alloys Part I: Influence of Nanocontainer Concentration

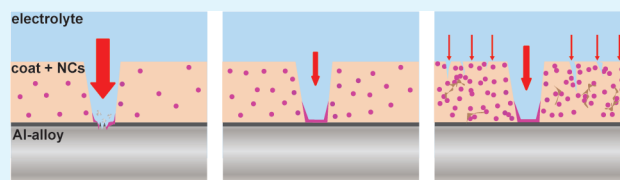
Dimitriya Borisova,* Helmuth Möhwald, and Dmitry G. Shchukin

Max Planck Institute of Colloids and Interfaces, Am Mühlenberg 1, 14424 Potsdam-Golm, Germany

Supporting Information

ABSTRACT: This work presents an effective anticorrosive coating for the industrially important aluminum alloy, AA2024-T3. The protective coating was designed by dispersing mesoporous silica nanocontainers, loaded with the nontoxic corrosion inhibitor, 2-mercaptobenzothiazole, in a hybrid sol-gel ($\text{SiO}_x/\text{ZrO}_x$) layer. The concentration of the embedded nanocontainers was varied (0.04–1.7 wt %) to ascertain the optimum conditions for anticorrosion performance. Attaining high efficiency was found to be a compromise between delivering sufficient corrosion inhibitor and preserving the coating barrier properties. The impact of nanocontainer concentration on the thickness and adhesion of freshly cured coatings was also investigated. The barrier properties of the intact coatings were assessed by electrochemical impedance spectroscopy. The active corrosion inhibition was evaluated during a simulated corrosion process by the scanning vibrating electrode technique. This study has led to a better understanding of the factors influencing the anticorrosion performance and properties of active anticorrosive coatings with embedded nanocontainers.

KEYWORDS: silica, nanocontainer, corrosion inhibitor, sol-gel, self-healing, aluminum alloy



INTRODUCTION

Corrosion of metal objects, such as machinery and vehicles, is a global problem with a significant environmental and economic impact.¹ Coatings are applied to corrosion-prone metals to inhibit corrosion in a passive or an active way. Standard anticorrosive coatings operate as a physical barrier between the metal and the corrosive environment. These coatings provide passive protection only when intact – if the coating is disrupted, the protection is compromised. In contrast, active protection utilizes the corrosion process as a trigger to induce corrosion inhibition, even when the protective layer is damaged. The most effective active corrosion inhibition of aluminum alloys is provided by conventional chromate conversion coatings.^{2,3} However, their toxicity and worldwide restriction creates an urgent need for finding effective corrosion preventing systems without the negative environmental impact of chromate.^{4–7}

Sol-gel technology is quite promising for the preparation of various environmentally friendly coatings with good adhesion to both metallic substrates and organic top coats.^{8,9} Their barrier properties are, however, restricted by pores and microcracks formed in the coating after curing. Embedding of nanoparticles in sol-gel derived coatings has been reported to improve the barrier properties of the sol-gel matrix.^{10,11} Unfortunately, these coatings act only as passive barriers and lose their protective function once they are damaged. Incorporation of corrosion inhibitors directly into sol-gel coatings offers a feasible way to provide active protection.^{12–14} However, these active coatings offer insufficient corrosion

resistance due to uncontrolled inhibitor release, loss of inhibition capability, and deterioration of the barrier properties of the sol-gel coatings.^{15,16}

A smart approach to overcome the drawbacks of the above-mentioned systems is the encapsulation of corrosion inhibitors in nanocontainers (NCs) dispersed in the matrix of the passive coating. The embedded NCs improve the physical barrier properties of the passive coating by lowering its porosity. In addition, NCs can be used to store a high amount of inhibitor and prevent its undesirable, prolonged interaction with the passive layer. Different encapsulation approaches have been reported so far, employing, for example, polymer containers,¹⁷ nanotubes,¹⁸ mesoporous inorganic materials,¹⁹ oxide nanoparticles,²⁰ NCs with polyelectrolyte shells²¹ and layered double hydroxides.²² The release of the encapsulated inhibitor is induced by environmental triggers such as changes in local pH, ionic strength or temperature; electromagnetic irradiation; and mechanical impact leading to cracks in the coating.²³

It was shown that sol-gel coatings incorporating metal oxide NCs loaded with organic corrosion inhibitor and coated with polyelectrolyte multilayers provide enhanced corrosion resistance.²⁴ These protective coatings are potential nontoxic alternatives to chromate conversion coatings and are also well-established for the Al-alloy, AA2024-T3. This alloy is extensively used in the aircraft industry, but is unfortunately

Received: February 14, 2012

Accepted: May 17, 2012

Published: May 17, 2012

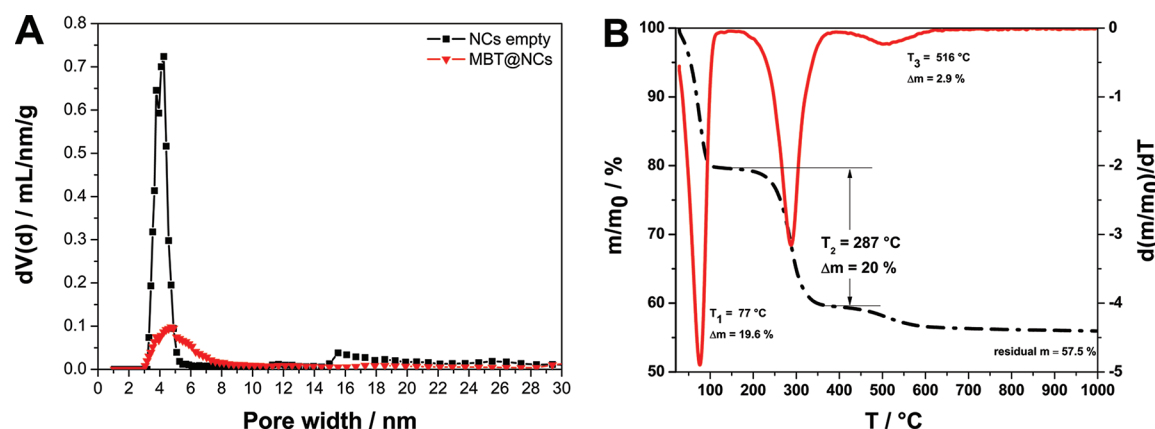


Figure 1. (a) pore size distributions from N_2 sorption measurements of mesoporous silica NCs: empty and containing MBT and (b) TGA results showing the mass loss of mesoporous silica NCs containing MBT.

very susceptible to localized pitting corrosion due to its intermetallic inclusions.^{25,26} Previous work in our group has focused on the use of less complicated NCs (e.g., halloysites or mesoporous silica NCs) loaded with corrosion inhibiting active agents. The active, anticorrosive coating systems incorporating these NCs were reported to exhibit increased corrosion resistance when applied on the AA2024-T3.^{27–29}

However, optimum corrosion inhibition can be obtained only after fulfilling certain technical requirements: (i) homogeneous dispersion of the embedded NCs; (ii) good adhesion and compatibility of the NCs and the coating matrix; and (iii) sufficient concentration of corrosion inhibitor. All these requirements are governed by the concentration of the embedded NCs. This, on one hand, should be as high as possible to provide sufficient inhibitor for active protection. On the other hand, a high NC content may deteriorate the barrier properties. Therefore, studying the complex dependence of coating performance on NC concentration is of great significance, especially considering the scarce works reporting on it.

This work describes the optimization of the performance of active anticorrosive coatings by tuning the concentration of the embedded NCs loaded with corrosion inhibitor. The investigated coating systems use mesoporous silica nanoparticles ($d \approx 80$ nm, $S_{\text{BET}} \approx 1000$ m² g⁻¹) as NCs because of their good compatibility with the applied SiO_x/ZrO_x sol–gel coating and their high capacity for inhibitor storage. The selected model inhibitor was the nontoxic 2-mercaptobenzothiazol (MBT), which is reported to be an effective corrosion inhibitor for the studied aluminum alloy, AA2024-T3.³⁰ Through studying the passive and active corrosion resistance of these systems, the optimum conditions for anticorrosion performance have been determined.

RESULTS AND DISCUSSION

Nanocontainers. Mesoporous silica nanocontainers (NCs) were synthesized following the protocol described in our previous work²⁹ and white stable colloidal water suspensions were obtained. The small polydispersity index (0.07), determined by dynamic light scattering (DLS), indicates good aqueous colloidal stability and narrow particle size distribution. SEM and TEM images (see Figure S1A, B in the Supporting Information) confirm the relative monodispersity and structural stability of the NCs. All NCs exhibit a spherical shape and diameters in the range between 60 and 80 nm, making their

incorporation in micrometer thick coatings easy. The TEM images reveal a well-developed pore structure. In all particles, the cylindrical pores are open, not ordered and oriented from the center to the outer surface, building a complex, wormlike pore system. N_2 sorption measurements showed a type IV isotherm with two closed hysteresis loops typical for mesoporous structures (see Figure S2 in the Supporting Information). The total surface area determined with the BET model is ~ 1000 m² g⁻¹, making the NCs promising hosts for the adsorption of guest molecules. NLDFIT (nonlocal density functional theory) modeling yields a cumulative pore volume of 1.2 mL g⁻¹ and a narrow pore size distribution with a distinct peak having a maximum at a pore diameter of 4 nm (Figure 1B).

The adsorption of the inhibitor, 2-mercaptobenzothiazole (MBT), at the NCs was conducted in ethanol under reduced pressure (50 mbar). This latter technique has previously been found to be beneficial in increasing loading.^{31–33} The quantity and decomposition temperature of the MBT incorporated in the NCs was determined using thermogravimetric analysis (TGA). The decomposition temperature of MBT was detected to be 288 °C (see Figure S3 in the Supporting Information). Thus, the 20% mass loss at 287 °C of the MBT loaded NCs, MBT@NCs (Figure 1A) can be attributed to the decomposition of MBT.

The incorporated MBT molecules change the porosity and surface area characteristics of the NCs. A reduction in the total pore volume and surface area is observed (see Figure S2 in the Supporting Information), indicating that the inhibitor molecules are adsorbed at the silica surface. The number of pores with an average diameter of 4 nm, which contribute the most to the calculated pore volume, is reduced after adsorption of the inhibitor molecules (Figure 1B). This suggests that the pores fill with MBT. A theoretical maximum loading capacity can be calculated by applying the density of MBT ($\rho_{\text{MBT}} = 1.42$ g mL⁻¹) and the pore volume of the empty silica NCs. Accordingly, 1 g NCs can contain a maximum of 1.7 g MBT, which is equal to a maximum loading capacity of 63 wt %. Therefore, the achieved experimental loading of 20 wt % is acceptable and a further increase in loading should be feasible. It should be noted that the high pore volume and large surface area of the investigated nontoxic NCs make them an attractive host material for different guest molecules. In contrast to comparable metal oxide NCs already reported in the literature, the NCs presented here possess much better encapsulating and

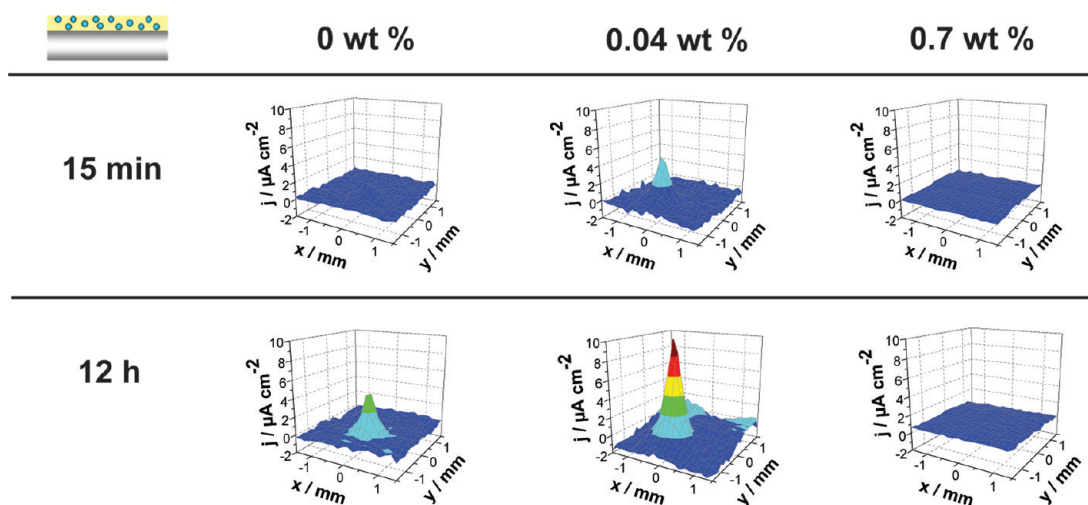


Figure 2. SVET 3D current density maps of aluminum (AA2024-T3) substrates coated with sol-gel coatings containing MBT@NC at different concentrations (0, 0.04, and 0.7 wt %). The systems shown are examples for detected high (for 0.04 wt %) and low (for 0.7 wt %) anodic current densities, in comparison to the control coating without MBT@NCs, after 15 min and 12 h immersion in 0.1 M NaCl.

storage properties, which could make them suitable for various applications, where high uptake and controlled delivery of encapsulated molecules are required.

Physical Properties of the Coatings. The model metal substrate used in this work (aluminum alloy AA2024-T3) was coated with a hybrid inorganic sol-gel ($\text{SiO}_x/\text{ZrO}_x$) doped with MBT@NCs using the dip-coating technique. The following concentrations of MBT@NCs, dispersed homogeneously in the final cured coatings, were studied: 0, 0.04, 0.1, 0.2, 0.5, 0.7, 0.8, and 1.7 wt %. These concentrations were chosen in order to preserve the integrity of the coating and to demonstrate that low concentrations of embedded NCs with high inhibitor loading offer sufficient passive and active corrosion resistance. The MBT@NCs were successfully dispersed in the sol-gel precursor solution and no precipitation of MBT@NCs was observed during the dip-coating of the metal plates. The thickness of the obtained coatings was measured on the AA2024-T3 surface with a coating thickness gauge using the Eddy-current principle.³⁴ The measured thicknesses of the different coating systems were in the range of 4 to 5 μm (see Figure S4 in the Supporting Information). The measurement accuracy is strongly influenced by the high roughness of the metal substrate as well as the low thickness of the coatings.

The surface of the cured, bare sol-gel film was investigated with scanning electron microscopy, which revealed that nanocracks developed in the passive sol-gel matrix after curing (see Figure S5 in the Supporting Information). This characteristic may have a negative impact on the barrier properties of the sol-gel coating.

The dry adhesion of the freshly cured coatings was determined using a pull-off test according to the standard method, ASTM D4541. An aluminum pull-stub with a diameter of 20 mm was first glued to the coating and then pulled off to remove the coating from the metal substrate. The pull-off force needed for detachment is divided by the test area to express adhesion as tensile stress. The results obtained for coatings with and without MBT@NCs are comparable, and are in the narrow range of 2–3 MPa (see Figure S6 in the Supporting Information).^{35–37} This finding means that incorporating MBT@NCs in the sol-gel matrix does not deteriorate the

adhesion between the coating and the metal substrate. Furthermore, the adhesion results are an indication for the good stability of the coatings with and without MBT@NCs. However, no well-defined correlation between adhesion and MBT@NC concentration could be determined.

Anticorrosive Properties of the Coatings. *Active Corrosion Resistance.* The active anticorrosive properties of the fabricated coating systems were evaluated in situ with the scanning vibrating electrode technique (SVET). This technique is ideal for the investigation of the coating performance on the aluminum alloy used in this work, because its high susceptibility toward localized corrosion, attributable to its intermetallic particles (IMPs) building galvanic couples with the surrounding matrix. An example of intermetallic particles are S-phase (CuMgAl_2) particles, which constitute $\sim 60\%$ of the IMPs¹³ and are present as micrometer sized grains dispersed within the whole Al matrix (see Figure S7 in the Supporting Information). These Cu and Cu-containing phases act as cathodes in the AA2024-T3 alloy, making the aluminum phase the anodic attack site. Thus, upon initiation of corrosion, a positive anodic and a negative cathodic current flow can be detected. Employing SVET, the electric field around a corrosion site is converted into an alternating voltage on the vibrating electrode tip, from which the current density can be calculated. As a result, the measured current density over an area can be plotted as a 3D current density map.^{3,38–40} By indicating the minimum and maximum current densities over the scanned area, a second plot can be drawn showing the change in current density with time.

In this study, the coated samples were scratched in a controlled way (see Materials and Methods) in order to accelerate the corrosion process and evaluate their active anticorrosive properties. In all samples, an anodic activity was measured above the scratch, which can be assigned to excess Al^{3+} ions produced by the oxidation and consequent dissolution of the aluminum metal. In the 3D maps, this process is expressed as a single positive peak with a constant position during the measurement, indicating that the anode is one defined pitting site (Figure 2). In contrast, no localized cathode was detected. Therefore, the poorly pronounced cathodic current that does not describe directly the metal oxidation was

not shown.⁴¹ The cathodic reaction generates OH^- ions, thereby increasing the local pH in the corroded area. These conditions are favorable for the dissolution of the inhibitor (MBT) molecules adsorbed on the embedded NCs.⁴² Accordingly, at the onset of corrosion, the inhibitor molecules are released and diffuse to the metal surface to form a protective layer preventing the direct contact of chloride anions with aluminum and its oxidation to Al^{3+} . As a consequence, an increase of the anodic current density with time can be assessed as a failure of the coating sample to inhibit corrosion evolution. In contrast, suppression of anodic activity is defined as self-healing. Therefore, the coatings inhibiting the corrosion processes in the scratched area are evaluated as being successful in active corrosion prevention.

The maximum anodic currents detected as a function of time are represented in Figure 3. A distinct corrosion propagation

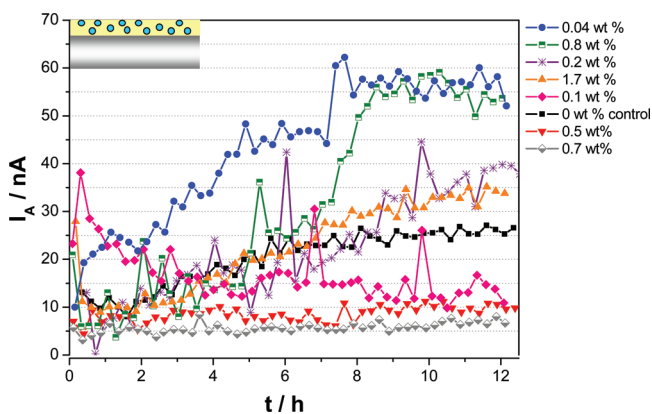


Figure 3. Maximum anodic currents detected with SVET over the scanned scratched area during a 12 h immersion period in 0.1 M NaCl. Results for coated samples containing different MBT@NC concentrations are shown.

expressed by the high values of anodic current, I_A (>30 nA) can be seen for samples with too high (0.8–1.7 wt %) and too low (0.04–0.2 wt %) MBT@NC concentrations. These samples reach anodic current values above that of the passive control system, suggesting poor active corrosion inhibition due to an insufficient inhibitor quantity in the case of low MBT@NC concentrations. The coatings with too high MBT@NC concentrations possess poor anticorrosive properties because of a possible deterioration of the passive layer due to more microdefects in the area neighboring the scratch, which are introduced by the higher amount of embedded NCs. Thus, based on the SVET study, a concentration window in which the corrosion process was inhibited successfully was determined to be between 0.5 and 0.7 wt %.

The SVET results are supported by the SEM micrographs depicting the scratched area after completion of the SVET tests. The high anodic activity detected by SVET for the control sample originates from an extensive corrosion attack. This is revealed by the formation and accumulation of a large amount of corrosion products covering the scratch in the sol–gel coating (Figure 4A). In addition, degradation of the integrity of the coating surrounding the scratch can be observed due to crevice (under-coating) corrosion. In contrast, the coating exhibiting the best active corrosion protection (0.7 wt % MBT@NCs) preserves its integrity and inhibits corrosion sufficiently. This is demonstrated by the defect-free and smooth

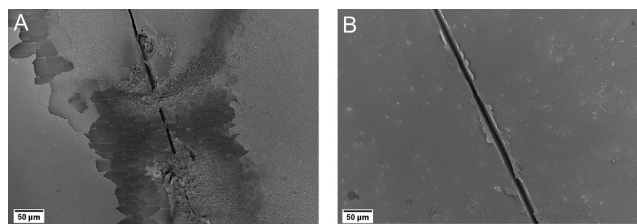


Figure 4. SEM micrographs of the scratched area after SVET analysis (12 h immersion in 0.1 M NaCl) of (a) the control (0 wt % MBT@NCs) and (b) the coated sample exhibiting lowest anodic current density (0.7 wt % MBT@NCs).

surface of the scratched area with no traces of corrosion products (Figure 4B).

Passive corrosion resistance. Electrochemical impedance spectroscopy (EIS) was used to evaluate the barrier properties and long-term corrosion resistance of the coated samples. The studied coatings functioning as pretreatments were directly exposed to a highly concentrated (1 M) NaCl solution without the deposition of additional layers (primer and top coat), which form an industrial final coating system. EIS spectra were collected over a time range of 14 days in order to understand the mechanism of ongoing corrosion and to quantify the anticorrosion performance of the studied coating. The dependence of the complex impedance on the applied frequency provides information about the capacitance and resistance of the different parts of the coating system. The deterioration of coating barrier properties and protective performance is revealed by an increase of capacitance, C , and decrease in resistance, R , resulting in a drop in the absolute impedance, $|Z|$.

The impedance spectra of the AA2024-T3 coated with intact sol–gel coatings containing different MBT@NC concentrations after 1 day immersion in 1 M NaCl are represented in the form of Bode plots in Figure 5. The phase angle spectra (Figure 5B) reveal two time constants (two maxima). The high frequency time constant (1×10^2 to 1×10^3 Hz) can be ascribed to the sol–gel coating capacitance (C_{coat}) and the low frequency time constant (1–10 Hz) to the capacitance of the intermediate oxide layer (Al–O–Si) at the metal-coating interface (C_{oxide}).⁴³ These elements of the coating system showed a resistive response, revealed by the two plateaus in the high (R_{coat}) and low (R_{oxide}) frequency regions (Figure 5A). The resistive parts of the sol–gel coating (R_{coat}) and intermediate oxide layer (R_{oxide}) result from pores and cracks in the coating system, as shown schematically in Figure 5C. As a result, sufficient coating barrier properties are revealed by good pore resistance resulting in high $|Z|$ values. Therefore, the two times higher $|Z|$ values measured after 1 day immersion for the coatings with 0.04, 0.7, and 1.7 wt % MBT@NCs account for better coating barrier properties (Figure 5A).

With immersion time, the aggressive electrolyte species diffused into the coating pores and led to further coating deterioration. Consequently, the formed defects at the coating-metal interface provided preferential pathways for the aggressive electrolyte ions to the metal substrate and caused the decrease of $|Z|$ measured after 7 days immersion (see Figure S8 in the Supporting Information). The further deterioration of the passive oxide layer resulted in metal dissolution and changes in the EIS spectra (Figure 6). Only one time constant at 10 Hz revealing the charge transfer processes in the corroded areas was detected (Figure 6B).⁴⁴ In addition, a new time

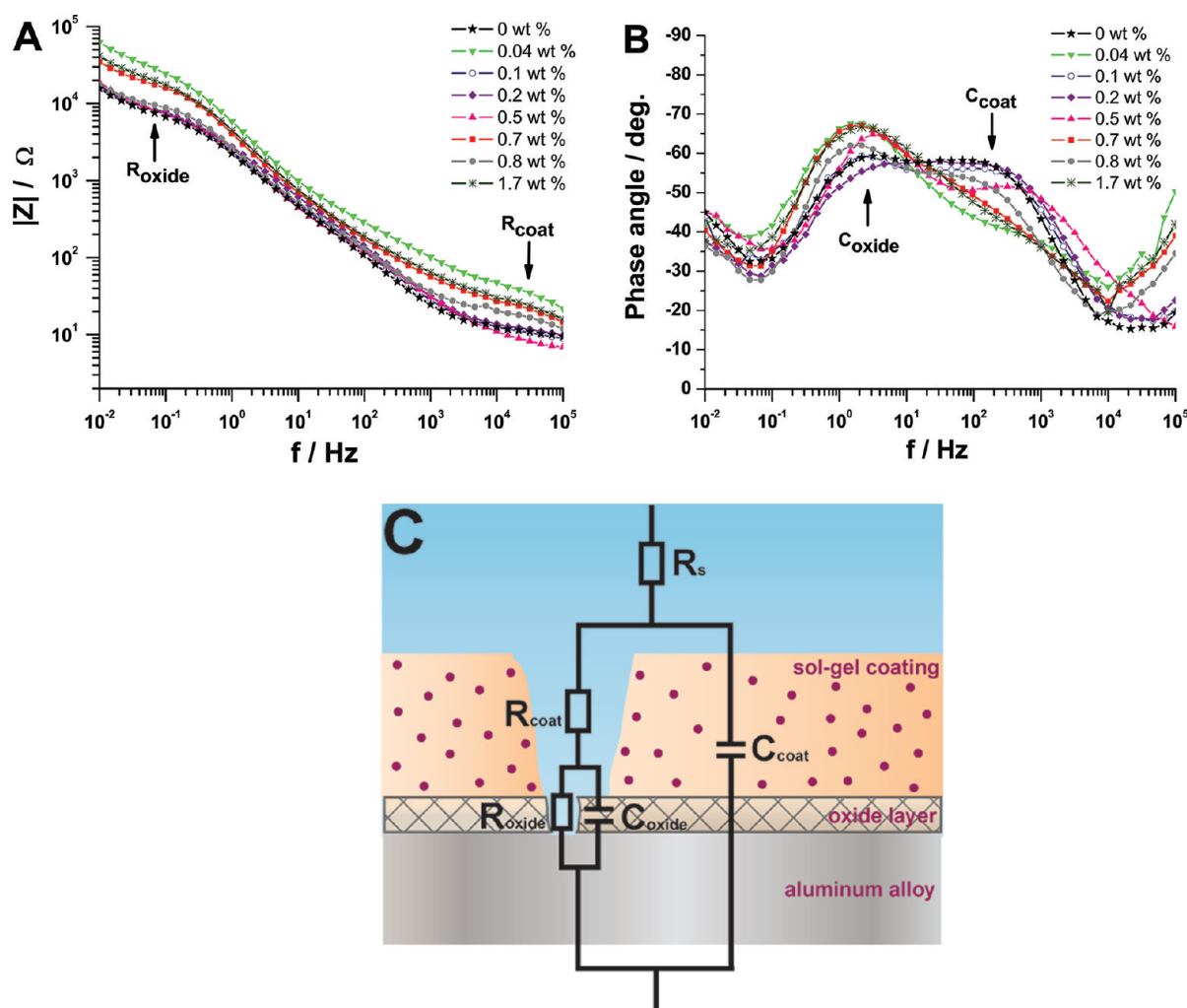


Figure 5. Bode plots showing the (a) absolute impedance and (b) phase angle as a function of frequency after 1 day immersion in 1 M NaCl of AA2024-T3 substrates coated with sol-gel coatings containing different MBT@NC concentrations; (c) a schematic representation of the parts of the coated samples and their corresponding equivalent circuit elements.

constant at 0.01 Hz was found, accounting for the diffusion controlled mass transfer of the corrosion products and corrosive agents diffusing to or from the metal surface.⁴⁵ Thus, after 14 days immersion in the highly concentrated (1M) NaCl solution, the detected electrochemical impedance response was dominated by the corrosion processes at the coating-metal interface as shown schematically in Figure 6C.

The Nyquist plots of all coated samples after 14 days immersion (Figure 7A) are characterized by a semicircle at high frequencies, corresponding to the charge transfer processes, and a straight line at low frequencies, representing the Warburg diffusion. Such Nyquist plots originate from electrochemical systems that can be represented by the Randles equivalent circuit (Figure 7A, inset), consisting of the solution (electrolyte) resistance (R_s), double layer capacitance (C_{dl}), charge transfer resistance (R_{ct}) and Warburg diffusion element (W).⁴⁶ The Warburg diffusion element represents the diffusion controlled mass transport of the corrosion products and the corrosive species. The double-layer capacitance and the charge transfer resistance characterize the corroded areas and contribute to the absolute impedance values in the low-frequency region.

Using this equivalent circuit (Figure 7A, inset), a numerical fitting of the measured EIS spectra after 14 days immersion was

performed. The calculated values of R_{ct} and C_{dl} for the studied coating systems after 14 days immersion in 1 M NaCl are presented in Figure 7B. High R_{ct} and low C_{dl} values reveal a limited electrolyte uptake and preserved barrier integrity. Therefore, all coating systems with resistances lower than that of the control coating without MBT@NCs demonstrate poor barrier properties resulting in insufficient corrosion resistance. The highest resistance value was obtained for the coating with 0.7 wt % MBT@NCs, followed by the coating with the lowest studied MBT@NC concentration (0.04 wt %). These coating systems also exhibit very low double layer capacitance values. In addition, they demonstrate the highest absolute impedance values in all frequency ranges during the whole EIS study. The incorporation of MBT@NCs at low concentrations (0.04–0.1 wt %) allows homogeneous dispersion of the NCs within the sol-gel matrix resulting in a better integrity and stability of the coating matrix. Furthermore, having fewer embedded NCs provides less interfacial area between the sol-gel matrix and the NC wall. Consequently, less diffusion paths are present in the coatings with low MBT@NCs concentration, which restricts the diffusion of aggressive electrolyte species toward the metal substrate. The good barrier properties of the coatings with higher MBT@NC concentrations can be explained by the higher amount of available

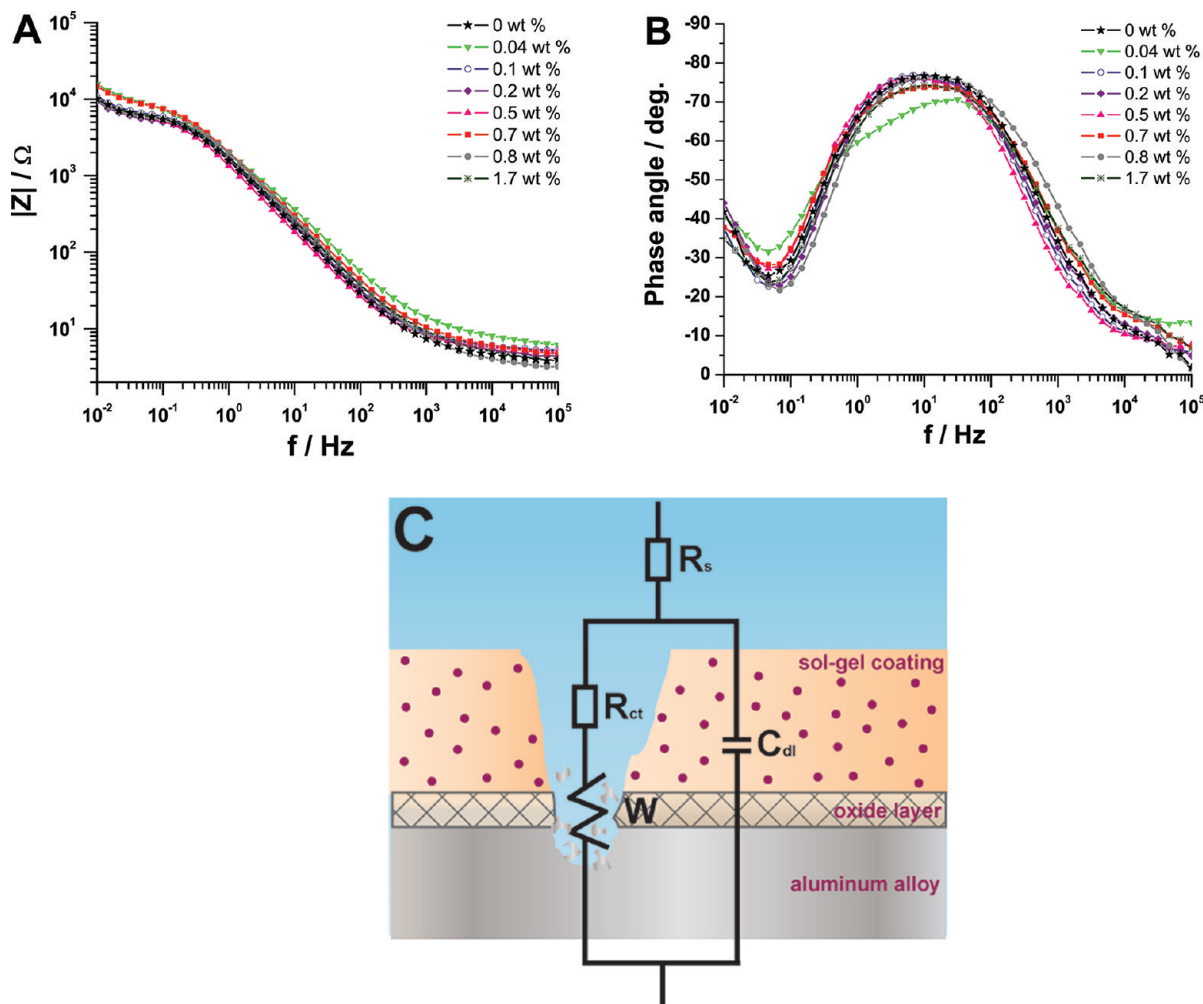


Figure 6. EIS data obtained after 14 days immersion in 1 M NaCl and represented as a Bode plot showing the change in (a) absolute impedance and (b) phase angle as a function of frequency for sol-gel coatings with different MBT@NC concentration; (c) a schematic representation of the equivalent circuit elements and their physical meaning.

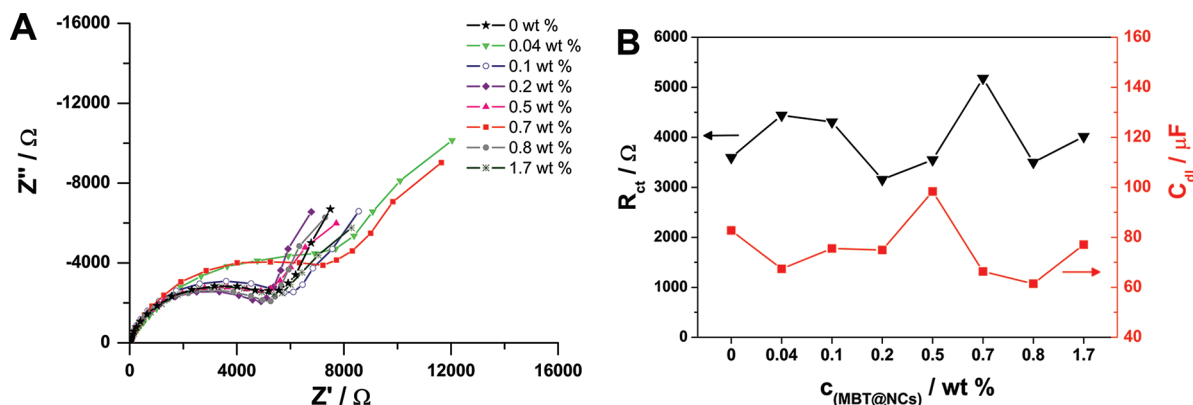


Figure 7. EIS data obtained after 14 days immersion in 1 M NaCl for sol-gel coatings with different MBT@NC concentrations: (a) experimental data represented as a Nyquist plot and (b) calculated data for the charge transfer resistance (R_{ct}) and double layer capacitance (C_{dl}) obtained after numerical fitting of the EIS spectra measured after 14 days immersion with the equivalent circuit shown in the inset.

inhibitor. The positive effect of the inhibiting species relies on their release upon the onset of corrosion. The released inhibitor molecules form a layer on the metal surface, which terminates the corrosion processes and restores partially also the coating barrier properties in the damaged coating area. In this study, higher inhibitor concentrations were achieved by using higher

MBT@NC concentrations in the coating. However, increasing the concentration of the embedded MBT@NCs above an optimum level (0.7 wt %) leads to poorer anticorrosion performance of the coating, as shown from the impedance data. This effect is due to the deterioration of the integrity and

barrier properties of the coating by possible agglomeration of the MBT@NCs embedded at higher concentrations.

A simple way to evaluate the barrier properties of the coating systems is by comparing the absolute impedance values at the lowest measured frequency ($|Z|_{0.01 \text{ Hz}}$) accounting for the corrosion resistance (Figure 8). The best coating performance

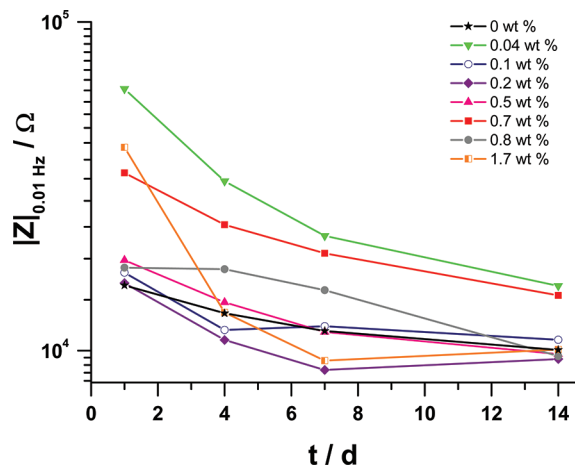


Figure 8. Measured absolute impedance values at 0.01 Hz over the course of the EIS study for the different intact coating samples immersed in 1 M NaCl.

over the whole course of the test is provided by the coatings with 0.04 wt % and 0.7 wt % MBT@NCs. These results reflect the ability of the NCs to passively preserve the coating integrity when introduced at very low concentrations and to actively improve the barrier stability by corrosion inhibition when embedded at sufficiently high concentrations. The EIS results are in good agreement with visual observation of the coated samples from photographs taken after 14 days immersion in 1 M NaCl (Figure 9). The dark pit-like defects and deposits of white corrosion products on the coating surface account for the extensive corrosion attack in the coatings with 0 and 1.7 wt % MBT@NCs. This excludes them from being viable coating systems providing long-term corrosion resistance. In contrast, a significantly less corrosion attack is observed for the coating with 0.04 wt % MBT@NCs, which also demonstrates good barrier properties in the EIS spectra. In addition, the areas in the coated samples, which are undamaged by corrosion, are intact and no coating cracks or delamination can be observed. This indicates good coating stability and sufficient adhesion to the metal even after 14 days immersion in 1 M NaCl.

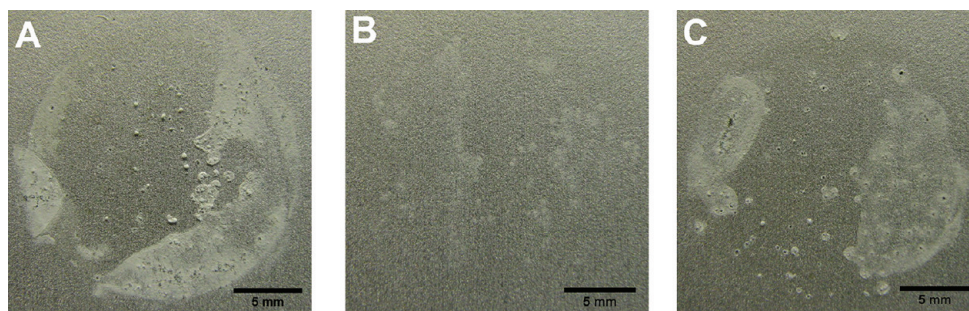


Figure 9. Photographs of the samples with sol-gel coatings containing (a) 0, (b) 0.04, and (c) 1.7 wt % MBT@NCs after 14 days immersion in 1 M NaCl.

CONCLUSIONS

In this work, we successfully embedded MBT loaded silica NCs (MBT@NCs) in a passive sol-gel layer to fabricate simple, active anticorrosive coating systems for the industrially important, corrosion-prone aluminum alloy, AA2024-T3. The high amount of nontoxic inhibitor (20 wt %) stored in the NCs was released upon corrosion attack to provide active, on-demand corrosion inhibition. The effect of the concentration of embedded NCs on the coating anticorrosion efficiency was determined to be a critical factor. It was found that incorporating MBT@NCs is not always favorable for the anticorrosion performance of the coating. Embedding MBT@NCs at very low concentrations (0.04 wt %) led to good coating barrier properties but no satisfactory active corrosion inhibition because of an insufficient amount of available inhibitor. In comparison, too high MBT@NC concentrations (0.8–1.7 wt %) deteriorate the coating integrity by introducing diffusion paths for aggressive electrolyte species, which results in a loss of anticorrosion efficiency. The best passive and active corrosion resistance was provided by the coating containing 0.7 wt % MBT@NCs, as determined with EIS and SVET analysis. This good anticorrosion performance is due to the preservation of the coating barrier properties and the sufficient inhibitor concentration (0.14 wt %).

Therefore, to obtain protective coatings with optimum anticorrosive properties, a compromise between coating integrity and active corrosion inhibition should be found.

MATERIALS AND METHODS

Materials. All chemicals used were commercially available and used without further purification. Tetraethyl orthosilicate (TEOS, $\geq 99\%$), hexadecyl trimethyl-ammoniumchloride (CTACl, 25% in H_2O), triethanolamine (TEA), and (3-glycidyloxypropyl) trimethoxysilane (GPTMOS, $\geq 98\%$) were purchased from Sigma-Aldrich. Ethyl acetoacetate (EAA) and zirconium(IV) propoxide solution (TPOZ, 70 wt % in 1-propanol) were purchased from Alfa Aesar. Nitric acid (HNO_3 , 65%) and hydrochloric acid (HCl, 37%) were supplied by Carl Roth. Sodium chloride (NaCl, analytical grade), sodium hydroxide (NaOH, 1 M) and 2-mercaptobenzothiazole (MBT) were obtained from Merck. Ethanol (EtOH) and propan-2-ol (IPA) were purchased from VWR Prolabo. The water used in all experiments was purified in a three-stage Millipore Milli-Q Plus 185 purification system. The aluminum alloy, AA2024-T3, used for corrosion testing was supplied by EADS Deutschland and cut into appropriate dimensions for the different analyses of the anticorrosive properties. For adhesion

tests, 3 M two component adhesive (Scotch-Weld DP 490) was used.

Synthesis Methods. Mesoporous silica NCs were synthesized following the protocol described previously.²⁹ Briefly, a mixture of TEOS/CTACl/TEA/H₂O/EtOH in the molar ratio of 1:0.27:1:137:6 was refluxed at 80 °C for 2 h. The template extraction was conducted in a HCl/ethanol mixture (15 mL HCl (37%):150 mL ethanol) for 30 min under ultrasonic agitation (Bandelin Sonorex Super 10P ultrasonic bath, 100 W, 35 kHz). The surfactant was separated by centrifugation (Beckmann L-70 ultracentrifuge, 49000 g, 20 min) and the solid cakes were repeatedly washed to obtain mesoporous silica NCs free of the template.

The subsequent loading of the silica containers with a corrosion inhibitor was conducted under reduced pressure (50 mbar). A silica-ethanol suspension (20 mg mL⁻¹) was mixed with an ethanol solution of 2-mercaptobenzothiazole (20 mg mL⁻¹) in 1:1 volume ratio and stirred for 4 h. The loaded containers (MBT@NCs) were separated by centrifugation and dried overnight at 60 °C.

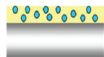
The hybrid SiO_x/ZrO_x sol for the subsequent dip-coating of the aluminum alloy (AA2024-T3) substrates was prepared using a sol-gel process, as reported by Zheludkevich et al.⁴⁷ The zirconium oxide sol was synthesized by hydrolyzing a 70 wt % zirconium(IV) propoxide (TPOZ) solution in propan-2-ol mixed with ethylacetoacetate (EAA) (volume ratio 1:1) at pH 0.5 (adjusted with HNO₃). The mixture was sonicated for 20 min to complex the precursor. The second organosiloxane sol was prepared by hydrolyzing (3-glycidyloxypropyl)-trimethoxysilane (GPTMS) in propan-2-ol and acidified water in a molar ratio (GPTMS/propan-2-ol/water) of 1:3:2. The formed zirconia-based sol was mixed by stirring with the organosiloxane sol in a 1:2 volume ratio. The final sol-gel mixture was placed in an ultrasonic bath for 60 min and then aged overnight at room temperature.

The aluminum substrates were chemically cleaned by immersion, first in 1 M NaOH for 15 min at 60 °C and then in 20 wt % nitric acid for 15 min at room temperature. Subsequently, the substrates were washed with Milli-Q water and dried with N₂ flow. Finally, the pretreated substrates were coated using a Bungard RDC 15 dip coater. The sol-gel films were produced by immersing the pretreated substrate in the respective sol-gel mixture for 100 s followed by controlled withdrawal at a speed of 2 mm s⁻¹. After coating, the samples were cured at 130 °C for 1 h.

Using the above method different coating systems were produced, depending on the concentration of MBT@NCs dispersed in the coating matrix. The following concentrations of MBT@NCs in the initial sol-gel mixture before curing were investigated: 0.25, 0.5, 1, 3, 4, 5, and 10 mg mL⁻¹. The weight loss during curing of the bare sol-gel coating was experimentally determined (by weighing coated substrates before and after curing) to be ~65%. The density of the wet, bare sol-gel was found by weighing a known volume to be approximately 0.9 mg mL⁻¹. Using this information, the concentrations of the particles in the final cured coatings were calculated to be 0.04, 0.1, 0.2, 0.5, 0.7, 0.8, and 1.7 wt % (see Chart 1).

Characterization Methods. The morphology, size and pore structure of the synthesized particles were characterized by transmission electron microscopy (Zeiss EM 912 Omega) with an accelerating voltage of 120 kV. Scanning electron microscopy (Zeiss Gemini LEO 1550) was employed to

Chart 1

Coating design	c(MBT@NCs) in cured coating [wt%]		c(MBT) in cured coating [wt%]	
	0	0.5	0	0.1
	0.04	0.7	0.008	0.14
	0.1	0.8	0.02	0.16
	0.2	1.7	0.04	0.34

analyze the silica samples as well as the coated metal substrates. An operating voltage of 3 kV and different magnifications were applied. N₂ sorption (Micromeritics TriStar 3000) at 77 K was used to study the porosity of the samples, which were baked under vacuum at 293 K prior to the measurements. The surface area and pore size distribution were obtained by applying the BET and NLDFIT models. Thermogravimetric analysis (NETZSCH TG 209 F1) was used to determine the quantity and decomposition temperature of the MBT incorporated into the NCs. The TGA measurements were conducted in an oxygen atmosphere (flow: 25 mL min⁻¹) and the weight change of the sample was detected while increasing the temperature (rate: 10 °C min⁻¹) in the range 25 to 1000 °C.

The coating thickness was measured with a coating thickness gauge, Surfex Pro S, from PHYNIX, Germany, using the Eddy-current principle. Electromagnetic induction was used to create a circulating (Eddy) current in the conducting aluminum substrate. Changes in the current flows induced by different coating thicknesses were detected using a coating thickness probe, FN1.5, attached to a stand and used in a nonferrous (FN) measuring mode.

The adhesion of freshly cured coatings to the Al-alloy substrates was measured following the standard test method, ASTM D4541. Self-aligning aluminum pull-stubs with a flat circular surface with diameter of 20 mm were glued to the coating surface with a two component adhesive and pulled off at a speed of 0.2 MPa s⁻¹ using an electronically controlled hydraulic pump (PosiTest AT-A, DeFelsko) to detach the coating from the metal surface.

The active anticorrosive properties of the coated samples were investigated in 0.1 M NaCl solution using the scanning vibrating electrode technique (SVET, Applicable Electronics). Prior to immersion in the NaCl solution, a controlled, straight scratch was made in the coating with a scalpel blade (Bayha blade No. 22) attached to a lever applying a controlled force. The scratch was deep enough to ensure exposure of the metal surface to the NaCl solution. SVET provided an in situ characterization of the corrosion process, which induces an electrostatic potential gradient inside the electrolyte solution leading to an alternating current signal. The vertical current density was recorded with the help of a vibrating PtIr electrode. The vibrating Pt-blackened electrode tip with a diameter of 20 μm was moved at a position 300 μm above the substrate on a lattice of 21 × 21 points over an area of 3 × 3 mm² (lateral step size: 150 μm). The vibration amplitude was 40 μm with a frequency of 864 Hz. The analyzed sample area was scanned within ca. 5 min and the scans were repeated every 15 min during the 12 h immersion period.

Electrochemical impedance spectroscopy (EIS) was employed to study the barrier properties of the intact coatings in 1 M NaCl solution at room temperature. The coated substrates (6 × 3 cm²) were placed into homemade cells, whereby a truncated area of 3 cm² of the sample was exposed to the salt solution. A three-electrode setup was used with impedance spectra being recorded at the corrosion potential, E_{corr} . A reference (saturated calomel) and a counter (platinum)

electrode were immersed in the cell. The coating at the edge of each sample was removed and the metal substrate, functioning as the working electrode, was connected to the potentiostat. The cell was placed in a Faraday cage and measurements were performed using a CompactStat electrochemical analyzer (Ivium Technologies). The current response was detected in the frequency range 0.01 Hz to 1 MHz at a constant potential (1 V). Six frequencies were typically assessed per decade. The amplitude of the sinusoidal voltage signal was 10 mV. The spectra were obtained and fitted using the software Ivium Soft (release 1.985). Digital photographs of the coated substrates after 14 days exposure to 1 M NaCl were captured with a Canon PowerShot S5 IS on super macro mode.

■ ASSOCIATED CONTENT

■ Supporting Information

Additional characterization data and Bode plots for coated samples (PDF). This material is available free of charge via the Internet at <http://pubs.acs.org>

■ AUTHOR INFORMATION

Corresponding Author

*E-mail: borisova@mpikg.mpg.de.

Notes

The authors declare no competing financial interest.

■ ACKNOWLEDGMENTS

We thank R. Rothe for BET analysis, M. Schenderlein for TGA measurements and J. Hartmann for SEM/EDX analysis. This work was financially supported by the ForMat program of the German Ministry for Science and Education (BMBF) and a German-Portuguese DAAD project.

■ REFERENCES

- (1) Schmitt, G.; Schütze, M.; Hays, G. F.; Burns, W.; Han, E.-H.; Pourbaix, A.; Jacobson, G.; World Corrosion Organization, http://www.corrosion.org/images_index/whitepaper.pdf (accessed May 2009).
- (2) Clark, W. J.; Ramsey, J. D.; McCreery, R. L.; Frankel, G. S. *J. Electrochem. Soc.* **2002**, *149*, B179.
- (3) He, J.; Gelling, V. J.; Tallman, D. E.; Bierwagen, G. P. *J. Electrochem. Soc.* **2000**, *147*, 3661.
- (4) EPA Federal Register: 1995; Vol. 60, p 45947.
- (5) Cohen, S. M. *CORROSION* **1995**, *51*, 71.
- (6) Twite, R. L.; Bierwagen, G. P. *Prog. Org. Coat.* **1998**, *33*, 91.
- (7) Hughes, A. E.; Cole, I. S.; Muster, T. H.; Varley, R. J. *NPG Asia Mater.* **2010**, *2*, 143.
- (8) Guglielmi, M. J. *Sol-Gel Sci. Technol.* **1997**, *8*, 443.
- (9) van Ooij, W. J.; Zhu, D. Q.; Prasad, G.; Jayaseelan, S.; Fu, Y.; Teredesai, N. *Surf. Eng.* **2000**, *16*, 386.
- (10) Gallardo, J.; Duran, A.; Garcia, I.; Celis, J. P.; Arenas, M. A.; Conde, A. J. *Sol-Gel Sci. Technol.* **2003**, *27*, 175.
- (11) Conde, A.; Durán, A.; de Damborenea, J. J. *Prog. Org. Coat.* **2003**, *46*, 288.
- (12) Raps, D.; Hack, T.; Wehr, J.; Zheludkevich, M. L.; Bastos, A. C.; Ferreira, M. G. S.; Nuyken, O. *Corros. Sci.* **2009**, *51*, 1012.
- (13) Galio, A. F.; Lamaka, S. V.; Zheludkevich, M. L.; Dick, L. F. P.; Müller, I. L.; Ferreira, M. G. S. *Surf. Coat. Technol.* **2010**, *204*, 1479.
- (14) Palanivel, V.; Huang, Y.; van Ooij, W. J. *Prog. Org. Coat.* **2005**, *53*, 153.
- (15) Garcia-Heras, M.; Jimenez-Morales, A.; Casal, B.; Galvan, J. C.; Radzki, S.; Villegas, M. A. *J. Alloys Compd.* **2004**, *380*, 219.
- (16) Voevodin, N. N.; Grebasch, N. T.; Soto, W. S.; Arnold, F. E.; Donley, M. S. *Surf. Coat. Technol.* **2001**, *140*, 24.

- (17) Latnikova, A.; Grigoriev, D. O.; Hartmann, J.; Möhwald, H.; Shchukin, D. G. *Soft Matter* **2011**, *7*, 369.
- (18) Lvov, Y. M.; Shchukin, D. G.; Möhwald, H.; Price, R. R. *ACS Nano* **2008**, *2*, 814.
- (19) Pomorska, A.; Yliniemi, K.; Wilson, B. P.; Shchukin, D.; Johannsmann, D.; Grundmeier, G. *J. Colloid Interface Sci.* **2011**, *362*, 180.
- (20) Snihirova, D.; Lamaka, S. V.; Taryba, M.; Salak, A. N.; Kallip, S.; Zheludkevich, M. L.; Ferreira, M. G. S.; Montemor, M. F. *ACS Appl. Mater. Interfaces* **2010**, *2*, 3011.
- (21) Shchukin, D. G.; Möhwald, H. *Small* **2007**, *3*, 926.
- (22) Wang, Y.; Zhang, D. *Mater. Res. Bull.* **2011**, *46*, 1963.
- (23) Shchukin, D. G.; Möhwald, H. *Chem. Commun.* **2011**, *47*, 8730.
- (24) Shchukin, D. G.; Möhwald, H. *Adv. Funct. Mater.* **2007**, *17*, 1451.
- (25) Boag, A.; Taylor, R. J.; Muster, T. H.; Goodman, N.; McCulloch, D.; Ryan, C.; Rout, B.; Jamieson, D.; Hughes, A. E. *Corros. Sci.* **2010**, *52*, 90.
- (26) Liu, Z.; Chong, P. H.; Butt, A. N.; Skeldon, P.; Thompson, G. E. *Appl. Surf. Sci.* **2005**, *247*, 294.
- (27) Fix, D.; Andreeva, D. V.; Lvov, Y. M.; Shchukin, D. G.; Möhwald, H. *Adv. Funct. Mater.* **2009**, *19*, 1720.
- (28) Hollamby, M. J.; Borisova, D.; Möhwald, H.; Shchukin, D. *Chem. Commun.* **2012**, 48.
- (29) Borisova, D.; Möhwald, H.; Shchukin, D. G. *ACS Nano* **2011**, *5*, 1939.
- (30) Harvey, T. G.; Hardin, S. G.; Hughes, A. E.; Muster, T. H.; White, P. A.; Markley, T. A.; Corrigan, P. A.; Mardel, J.; Garcia, S. J.; Mol, J. M. C.; Glenn, A. M. *Corros. Sci.* **2011**, *53*, 2184.
- (31) Lu, J.; Liang, M.; Zink, J. I.; Tamanoi, F. *Small* **2007**, *3*, 1341.
- (32) Cauda, V.; Schlossbauer, A.; Kecht, J.; Zürner, A.; Bein, T. *J. Am. Chem. Soc.* **2009**, *131*, 11361.
- (33) Vallet-Regí, M.; Balas, F.; Arcos, D. *Angew. Chem.* **2007**, *119*, 7692.
- (34) Kral, J.; Smid, R.; Ramos, H. M. G.; Ribeiro, A. L. In *2011 Instrumentation and Measurement Technology Conference (I2MTC); IEEE: Piscataway, NJ, 2011*; p 1.
- (35) Rickerby, D. S. *Surf. Coat. Technol.* **1988**, *36*, 541.
- (36) Mohler, J. B. *Met. Finish.* **1983**, *81*, 71.
- (37) ASTM Standard D4541: Standard Test Method for Pull-Off Strength of Coatings Using Portable Adhesion Testers; ASTM International: West Conshohocken, PA, 2009; 10.1520/D4541-09E01.
- (38) Pratt, K. W., Jr.; Johnson, D. C. *Electrochim. Acta* **1982**, *27*, 1013.
- (39) Isaacs, H. S.; Davenport, A. J.; Shipley, A. J. *Electrochem. Soc.* **1991**, *138*, 390.
- (40) Worsley, D. A.; McMurray, H. N.; Belghazi, A. *Chem. Commun.* **1997**, 2369.
- (41) Fix, D.; Skorb, E. V.; Shchukin, D. G.; Möhwald, H. *Meas. Sci. Technol.* **2011**, *22*.
- (42) Woods, R.; Hope, G. A.; Watling, K. J. *Appl. Electrochem.* **2000**, *30*, 1209.
- (43) Grundmeier, G.; Schmidt, W.; Stratmann, M. *Electrochim. Acta* **2000**, *45*, 2515.
- (44) Zheludkevich, M. L.; Shchukin, D. G.; Yasakau, K. A.; Möhwald, H.; Ferreira, M. G. S. *Chem. Mater.* **2007**, *19*, 402.
- (45) Zheludkevich, M. L.; Serra, R.; Montemor, M. F.; Yasakau, K. A.; Salvado, I. M. M.; Ferreira, M. G. S. *Electrochim. Acta* **2005**, *51*, 208.
- (46) Chang, B.-Y.; Park, S.-M. *Annu. Rev. Anal. Chem.* **2010**, *3*, 207.
- (47) Zheludkevich, M. L.; Serra, R.; Montemor, M. F.; Salvado, I. M. M.; Ferreira, M. G. S. *Surf. Coat. Technol.* **2006**, *200*, 3084.